Case Study

Nondestructive Assessment of Axial Load–Deflection Behavior of Drilled Shafts for a Suspension Bridge

Federico Pinto[1]; Carlos F. Gerbaudo[2]; and Carlos A. Prato[3]

Abstract: The new Río Cuarto Bridge, currently under construction in the Province of Córdoba, Argentina, consists of a 110-m long, cable-stayed main span with a prestressed concrete deck, steel pylons, and two 50-m–long side spans founded on groups of drilled shafts. The construction method, structural configuration of the superstructure, and post-tensioning sequence of the cables required a detailed characterization of the axial load behavior of the drilled shafts, both for the temporary support shafts and the foundation piers. Small-strain and working load level predictions were made during design, on the basis of conventional site investigation information and in situ geophysical testing. A series of nondestructive evaluations, coupled with nonlinear extrapolations calibrated to represent the measured small-strain range, were carried out in lieu of conventional verification of design predictions by means of more cumbersome large-strain testing. The testing program consisted on monitoring accelerations generated at the top of the shaft as a result of a small amplitude dynamic load measured by means of a dynamic force transducer. A nonlinear numerical model was then calibrated so as to reproduce the initial stiffness measured during the small-strain testing program to extrapolate the load-deflection curve into the service load range and thus define load-deflection curves of the shafts at each pier location up to service load levels. To obtain an experimental validation of the approach at the site, a conventional static load test, carried up to the service load level, was performed on a main pier shaft. Results showed a reasonable agreement between the nondestructive evaluation with nonlinear extrapolation, large-strain measurements, and design predictions for the main pier shafts, whereas some differences were observed between the design predictions and small-strain measurements at other locations, primarily as a result of as-built conditions unforeseen in the original design. Thus, the nondestructive testing program was instrumental in the verification of the as-built behavior of the shafts and allowed the development of load-deflection curves for the drilled shafts that accurately represented the behavior up to the service load level. **DOI: 10.1061/(ASCE)IS.1943-555X.0000059.**

CE Database subject headings: Drilled shafts; Dynamic tests; Stiffness; Nondestructive tests; Suspension bridges; Axial loads; Deflection.

Author keywords: Drilled shafts; Dynamic testing; Stiffness; Nondestructive evaluation.

Introduction

The determination of load-deflection curves of as-built drilled shafts for major civil infrastructure works into the service load range frequently warrants large-strain testing of either production or test shafts (Reese and O'Neill 1988). On the other hand, low-strain, nondestructive testing (NDT) is also routinely performed in these elements to provide quality control of the work, regarding structural integrity of the shafts and stiffness of the concrete. Given the fact that large-strain tests are normally expensive and that they may be regarded as "destructive" to a certain extent, a nondestructive technique that could serve both for integrity testing and for deriving load-deflection curves equivalent to those derived by means of large-strain testing would provide several advantages compared with conventional testing programs.

Such a technique has been proposed by Caballero et al. (2003) and Caballero (2006) by means of applying and measuring a small amplitude impulsive force using an instrumented hammer and measuring the transient response at the top of the shaft. The test is repeated a few times, and after a signal processing technique to minimize noise, as described subsequently, an accurate measurement of the small-strain vertical stiffness of the element is obtained. Using a nonlinear numerical model, calibrated to represent the accurately measured initial stiffness, and recognizing that the initial stiffness dominates the behavior within the service load range as a result of the large factors of safety normally considered in design (AASHTO 2008), a load-deflection curve extrapolated into the nonlinear range is obtained by means of the model considering soil properties obtained during the site exploration program for the design.

This paper presents an application of the proposed technique for a major bridge work in the province of Córdoba, Argentina; conventional static load testing (SLT) was also performed, providing a unique opportunity to test the approach and to assess the accuracy of design predictions on the basis of well-accepted engineering calculation methods.

Río Cuarto Bridge

The Río Cuarto Bridge consists of a cable-stayed superstructure with prestressed concrete deck and metallic pylons, with a main span of 110 m, two side spans of 50 m, and access viaducts in both

[1]Dept. de Estructuras, Univ. Nacional de Córdoba, FCEFyN Córdoba, Argentina (corresponding author). E-mail: fpinto@efn.uncor.edu

[2]INGROUP Oficina de Proyectos, Dept. de Estructuras, Univ. Nacional de Córdoba, FCEFyN, Córdoba, Argentina.

[3]Dept. de Estructuras, Univ. Nacional de Córdoba, FCEFyN Córdoba, Argentina.

Note. This manuscript was submitted on January 12, 2010; approved on April 7, 2011; published online on February 15, 2012. Discussion period open until August 1, 2012; separate discussions must be submitted for individual papers. This paper is part of the ***Journal of Infrastructure Systems***, Vol. 18, No. 1, March 1, 2012. ©ASCE, ISSN 1076-0342/2012/1-0–0/$25.00.

margins. All piers are founded on groups of drilled shafts, with lengths that range from 20 to 28 m. The construction procedure of the superstructure requires the installation of temporary shafts, which are to provide support to the bridge deck before the installation and tensioning of the cable stays. Once the bridge deck is fully assembled, the cable stays are installed and put in tension, after which the temporary shafts are demolished.

Fig. 1 shows a schematic view of the bridge; the suspended portion of the structure is supported by two main piers (P5 and P6), two intermediate piers (P4 and P7), and two retention piers (P3 and P8). The main piers are founded on two groups of 12 drilled shafts, 0.80 m in diameter (Fig. 2), whereas the intermediate piers are founded on two 1.20-m–diameter shafts. The retention piers, which are to sustain tension loads under certain conditions, are founded on two groups of four drilled shafts, 0.80 m in diameter. The south and north viaducts are supported on 1.0-m–diameter column shafts, whereas the temporary support shafts are 0.90 m in diameter.

The construction sequence and the final performance of the structure are significantly affected by possible settlements of the foundations, for which an accurate characterization of the axial load–displacement behavior was warranted during design on the basis of design soil properties derived by means of a conventional site investigation program and geophysical information available at the site.

Site Conditions

The bridge spans across the riverbed and floodplains of the Río Cuarto River (Fig. 3), which shows typical meandering features of a plain river. A site investigation program was carried out consisting of six standard penetration test (SPT) borings, from which samples were retrieved to perform laboratory identification and strength testing at several locations and depths within the site. Fig. 3 shows the typical soils encountered, consisting of a scourable top layer of coarse sand with thickness ranging from 3 to 7 m, followed by a deep layer of low-plasticity silt and clay, with occasional pockets of sand layers. Typical SPT blow counts start at $N = 10$ blows per foot (bpf) for surficial soils, increasing to $N = 30$ bpf for soils at depths of 20 m (approximate), indicating a steady increase in density and stiffness with depth.

A complementary in situ geophysical test was performed to derive the small-strain stiffness variation of the soils with depth. Several techniques were considered, but because of access and schedule restrictions, the Spectral Analysis of Surface Waves (SASW) technique (Stokoe et al. 1994) was employed. This technique, which operates entirely from the surface of the soil deposit, was performed within the vicinity of pier P6. The testing was carried out such that a shear wave velocity profile was derived down to a depth of 25 m. Information on the small-strain stiffness profile was also available at a nearby location along the river, showing very similar conditions to the bridge crossing, thus indicating little spatial variability, consistent with the geology of the site. Fig. 4 shows the small stiffness variation with depth; there is a steady increase with depth, with an observed shear wave velocity $Vs = 150$ m/s near the surface and $Vs = 500$ m/s for depths greater than 12 m, consistent with the SPT blow count trends obtained at all boring locations.

Design Predictions

Small-Strain Stiffness

Small-strain stiffness of drilled shafts was evaluated during the design phase of the project on the basis of the SASW testing results. The evaluation followed Randolph and Wroth's (1978) load transfer theory, which has been shown to agree well with

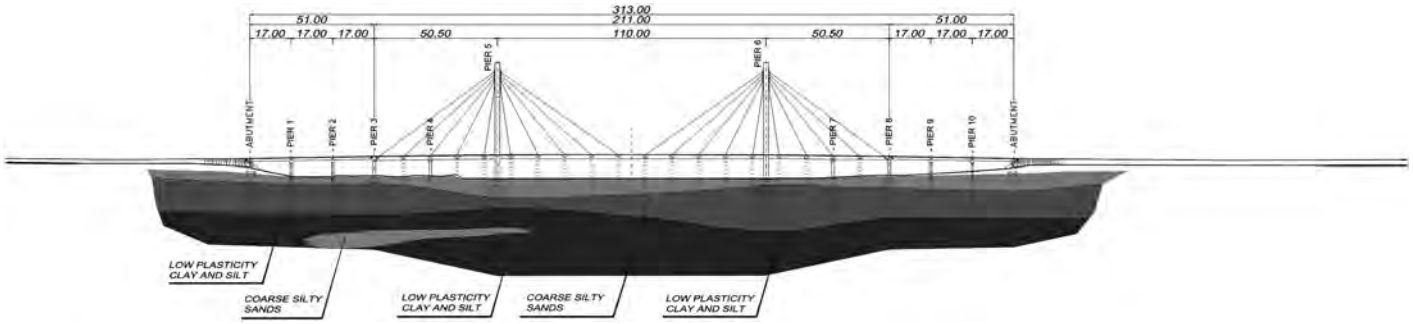

Fig. 1. Layout of Río Cuarto Bridge and subsurface conditions

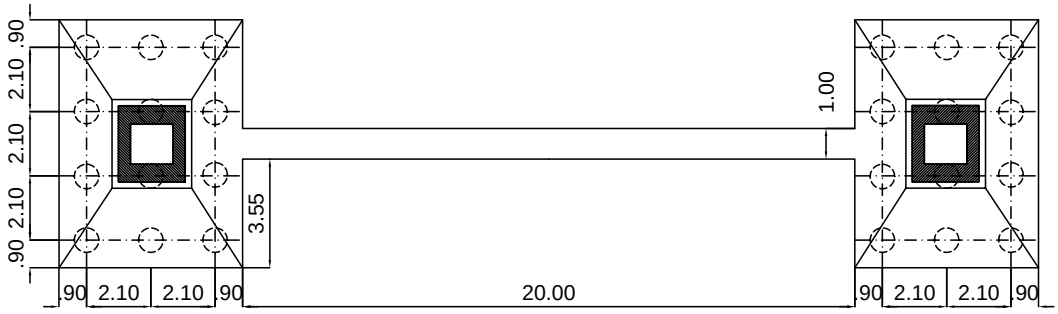

Fig. 2. Main pier foundations of Río Cuarto Bridge

Fig. 3. View of bridge structure (image by Federico Pinto; Carlos F. Gerbaudo; and Carlos A. Prato)

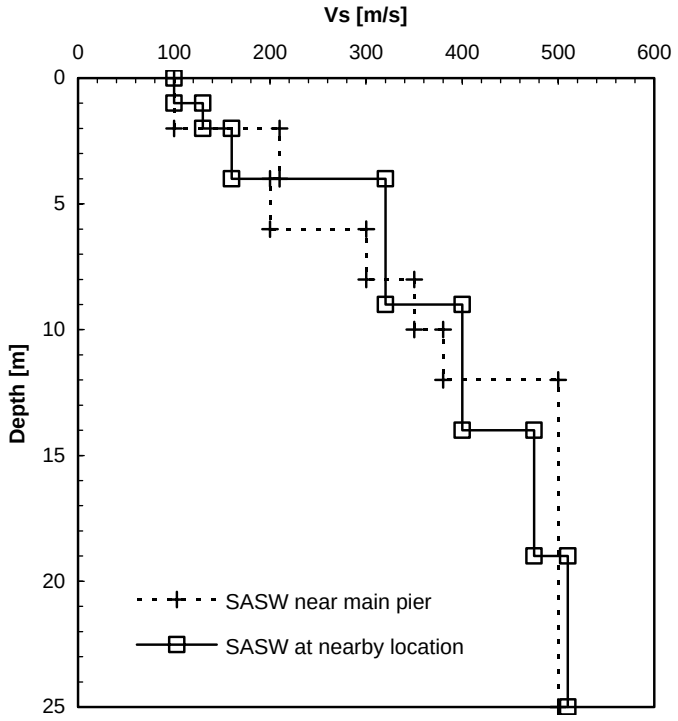

Fig. 4. Shear wave velocity profile at site derived by means of Spectral Analysis of Surface Waves method

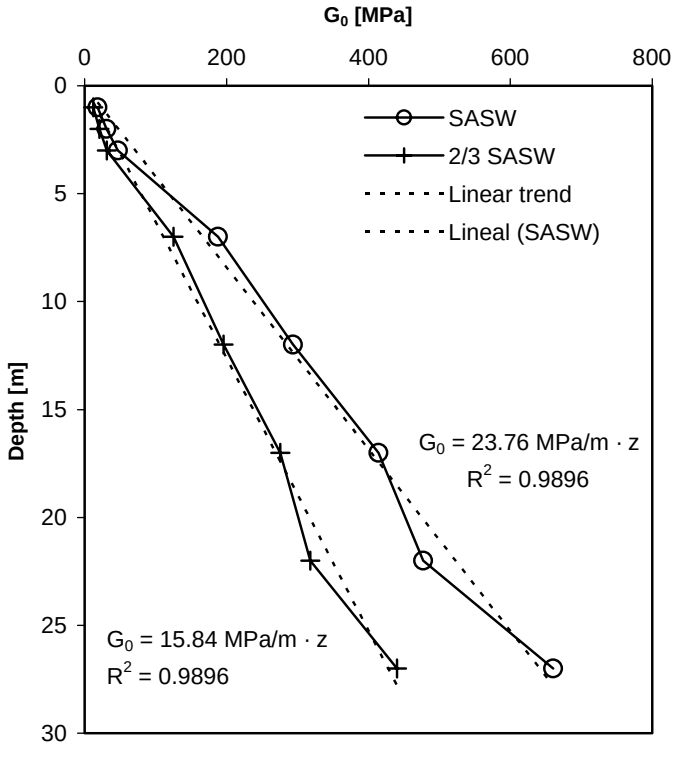

Fig. 5. Design small-strain stiffness profile

more-sophisticated rigorous boundary element analyses (Pinto and Prato 2006). With the exception of the auxiliary pier shafts, the analysis did not account for underreams at the bottom, which were not included in the original design.

On the basis of the small-strain stiffness profile derived by means of the SASW tests (Fig. 3), two design profiles were evaluated; one corresponded to undisturbed soil conditions, in which a linear variation of shear stiffness G_0 with depth is adopted, and another profile had a two-thirds reduction in stiffness with respect to undisturbed conditions to account for possible disturbance effects during installation of the shafts (Fig. 5). Conservative design predictions were made on the basis of the reduced stiffness profile.

Table 1 shows small-strain stiffness predictions for different pier locations, considering both undisturbed and reduced soil stiffness. The Young's modulus of concrete considered for the stiffness calculations was $E = 30$ GPa.

The two-thirds reduction in soil stiffness has a significant (although not linear) effect on the axial stiffness evaluation; the undisturbed values are approximately 26% greater than the estimates on the basis of reduced soil stiffness.

Although not anticipated in the original design, drilled shafts at several locations were constructed with underreams. The presence of underreams would be expected to have little effect on the initial stiffness of long shafts ($L > 25D$, in which $L =$ length and $D =$ diameter), particularly for load levels that are below the friction capacity of these elements. Nevertheless, Table 2 shows a comparison of the expected effect of the underreams in the initial stiffness, in which the effect, although modest (approximately 10%), is still noticeable.

Table 1. Design Initial Stiffness Estimates

Piers	Dimensions (m)	Reduced stiffness (kN/mm)	Intact stiffness (kN/mm)
Main piers (P5,P6)	$L = 28$; $D = 0.8$	1,950	2,460
Intermediate piers(P4, P7)	$L = 22.5$; $D = 1.2$	2,760	3,480
Retention piers (P3, P8)	$L = 21.3$; $D = 0.8$	1,720	2,160
Auxiliary pier (AP11)	$L = 11$; $D = 0.9$	1,520	1,970
Auxiliary pier (AP15)	$L = 15$; $D = 0.9$, 1.3 underream	1,800	2,290

Table 2. Effect of Underream on Initial Stiffness Estimates

Piers	Underream diameter (m)	Intact stiffness without underream (kN/mm)	Intact stiffness—with underream (kN/mm)
Intermediate piers (P4, P7)	1.6	3,480	3,730
Retention piers (P3, P8)	1.2	2,160	2,380

Nonlinear Predictions

The axial load–deflection curves of the shafts were derived during design by means of the $t - z$ curves proposed by Reese and O'Neill (1988). These curves, which are prescribed as an analysis tool for settlement estimates in several bridge design manuals (AASHTO 2008), show the variation of the axial reaction of the shaft per unit length, t, as a function of the shaft settlement z. Reese and O'Neill (1988) present curves for both clayey and sandy soils. Because the soils at the site consist of low -plasticity clays and silts, curves for both clays and sands are considered for preliminary evaluations.

The $t - z$ curves presented by these authors are given as a range of values normalized by shaft diameter z/D and ultimate skin friction t/t_u. Figs. 6 and 7 show normalized soil reaction versus settlement curves, in which there is large uncertainty associated with the response for the small-strain range for both clay and sandy soils, respectively. It should also be pointed out that Reese and O'Neill (1988) define a conventional end bearing failure at a tip settlement of 5% of the shaft diameter.

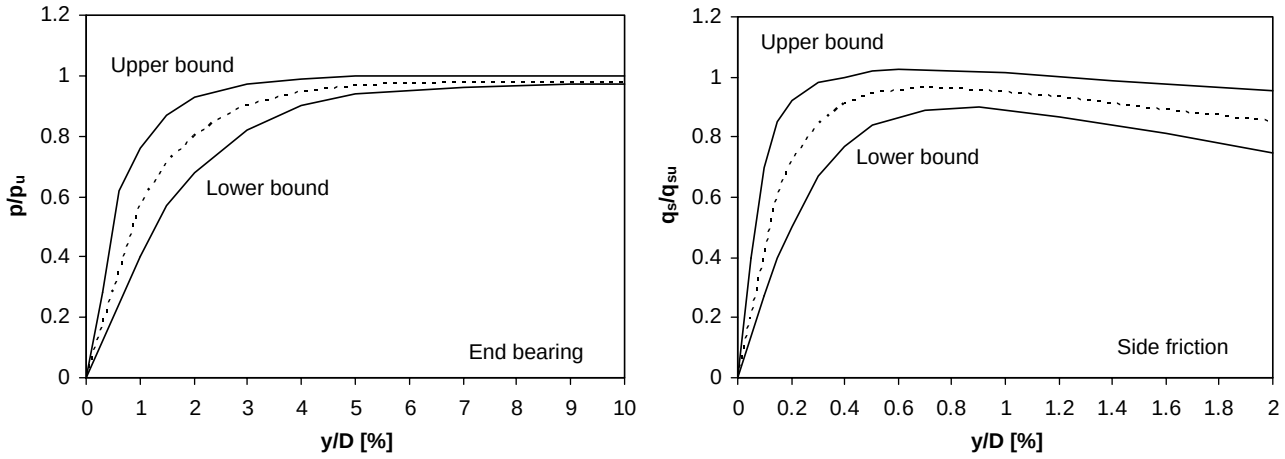

Fig. 6. $t - z$ Curves for drilled shafts on clay (Reese and O'Neill 1988)

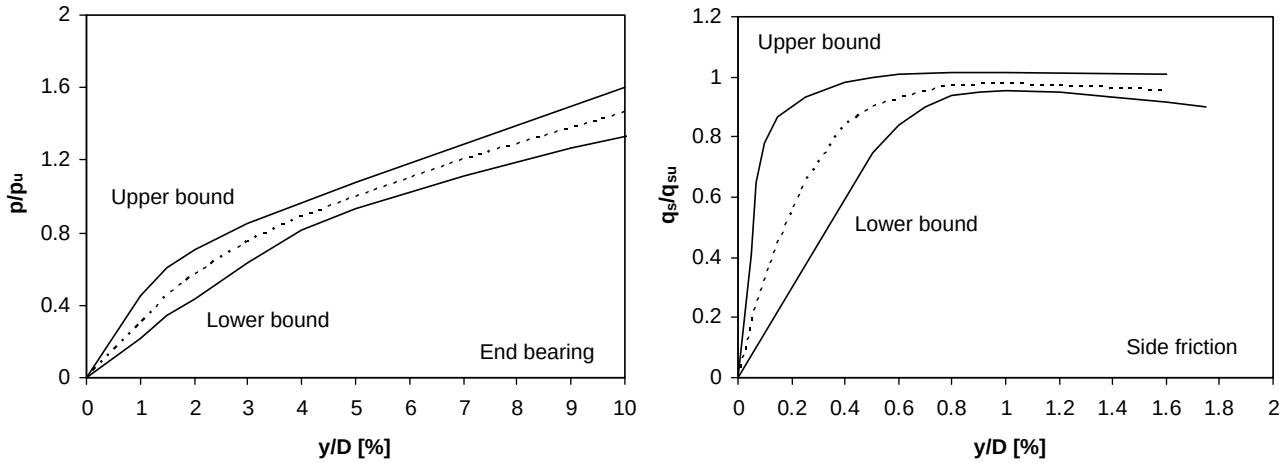

Fig. 7. $t - z$ Curves for drilled shafts on sand (Reese and O'Neill 1988)

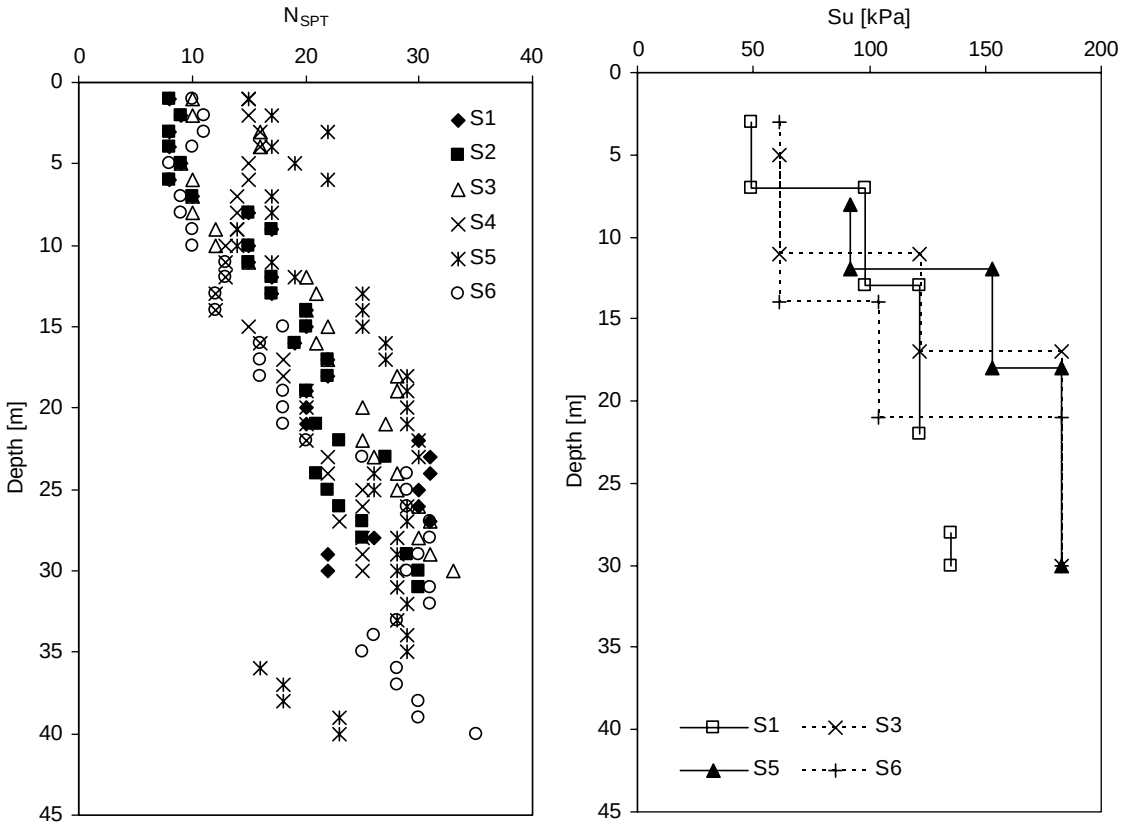

Fig. 8. Soil strengths at site from in situ and laboratory tests

Fig. 8 shows the undrained shear strength s_u, and SPT blow count N_{SPT} profiles determined on the basis of laboratory and in situ SPT testing. Ultimate end bearing and skin friction values are obtained on the basis of the strength information shown on Fig. 8, following Reese and O'Neill's (1988) method. Thus, nonlinear springs are defined to model the soil reaction along the pile and at the tip considering the normalized curves in Figs. 6 and 7 and the ultimate bearing values on the basis of the soil properties shown in Fig. 8.

Considering linear material behavior for the shaft and the nonlinear springs, a numerical model is set up to derive the axial load–deflection behavior of the shafts, without accounting for possible group effects, which are later assessed in the design. Load-deflection curves are derived for lower-bound, average, and upper-bound spring estimates. Fig. 9 shows the load-deflection curves obtained for a main pier (P6) shaft, assuming claylike and sandlike soil response. The the average trends are very similar. Because the site characterization indicates that soils are plastic, the clay curves are considered for design.

Given the fact that the small-strain stiffness is not well represented by the $t - z$ curves, as shown in Fig. 10 for a main pier shaft, the load-deflection curves are adjusted by linear interpolation between the initial stiffness prediction and the $t - z$ curve prediction such that the load-deflection curve matches the $t - z$ curve prediction at displacements that are approximately 0.1% of the shaft diameter. This value is chosen on the basis of the fact that the skin friction resistance appears to be frankly non-linear after this settlement, as shown on Figs. 6 and 7.

For a service load of 2,150 kN per shaft at the main pier P6, the estimated settlement in Fig. 10 is approximately 2.3 mm.

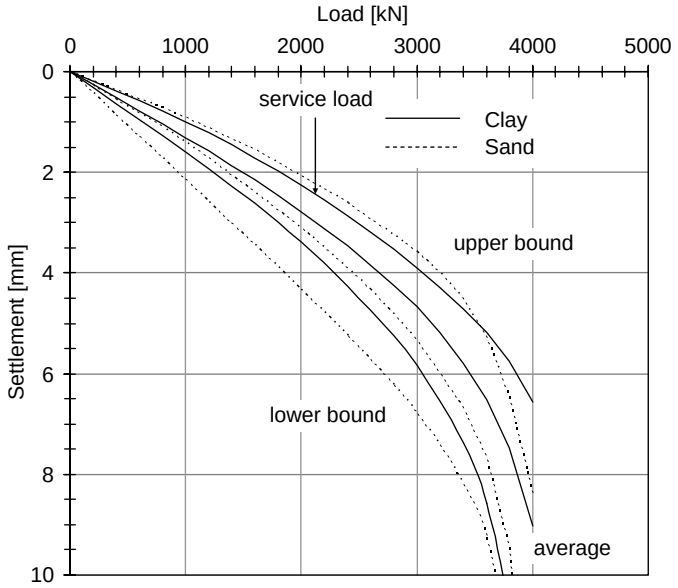

Fig. 9. Load-deflection curves at main pier (P6) without small-strain stiffness adjustment

Testing Program

A nondestructive pile testing program was set up to obtain an experimental verification of the design predictions and the integrity of the as-built shafts. The program consisted of small-strain integrity

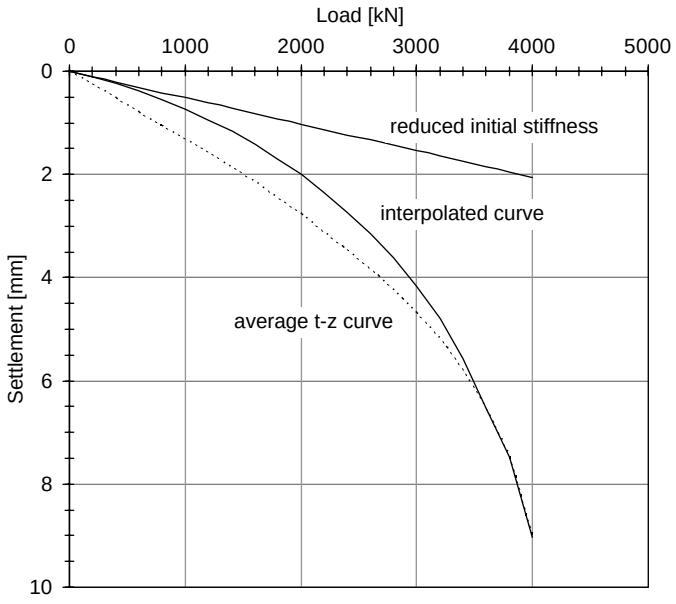

Fig. 10. Load-deflection curve at main pier (P6) with small-strain stiffness adjustment

tests (impact echo), small-strain dynamic tests, and a conventional SLT carried up to service loads to validate the nonlinear extrapolations on the basis of the small-strain measurements. This presents on the small-strain test dynamic and SLT performed to assess axial load behavior, and the integrity tests are not discussed.

Small-Strain Testing

The primary goal of these tests was to obtain an experimental verification of the as-built initial stiffness of the shafts by means of accurate small-strain measurements. The experimental technique, described in detail by Caballero et al. (2003) and Caballero (2006), consisted of applying a dynamic load at the top of the shafts by means of an instrumented hammer and registering the response at the top of these elements (Fig. 11). The load is developed by means of a 50-kg mass falling from a 1.0-m height, with a spring-dashpot system attached at the tip of a rod connected to the falling mass. The loading history and the shaft response in terms

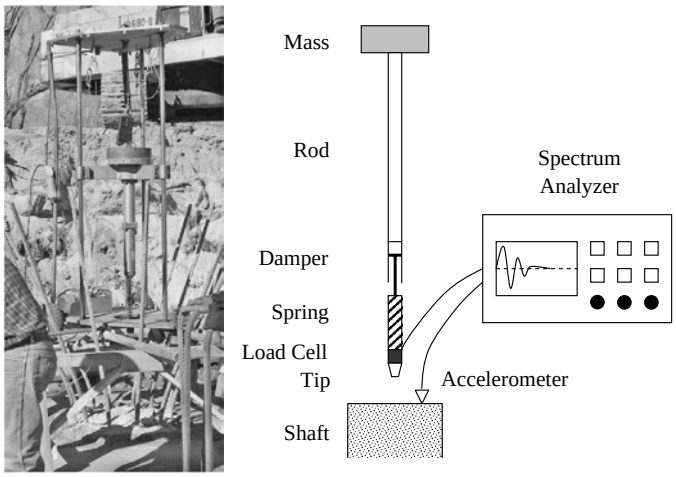

Fig. 11. Layout of small-strain dynamic pile tests (image by Federico Pinto; Carlos F. Gerbaudo; and Carlos A. Prato)

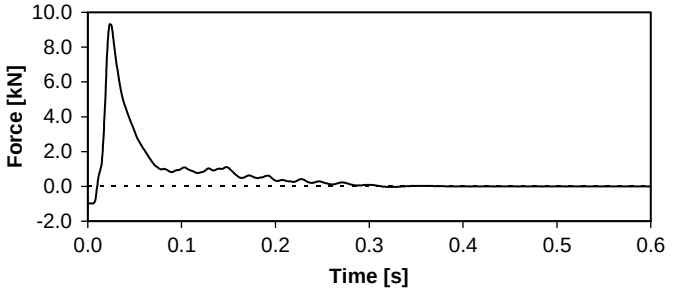

Fig. 12. Impact force history of small-strain dynamic pile test at main pier (P6)

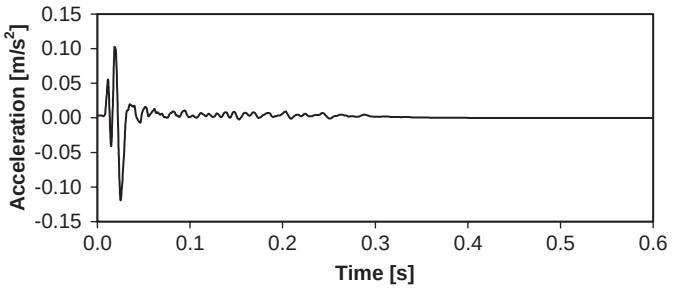

Fig. 13. Acceleration history at pile head during small-strain dynamic pile test at main pier (P6)

of head accelerations are recorded by means of a digital spectrum analyzer.

Ten records of load and acceleration histories at the top of the shafts are obtained to minimize the effects of ambient and instrumental random noise. Figs. 12 and 13 show typical force and acceleration records for a main pier shaft, in which the load peaks at approximately 12 kN, with a total duration of approximately 0.3 s. The acceleration records show a maximum of 0.12 m/s^2 and higher-frequency content than the input load.

The frequency range at which measurements are consistent and signal-to-noise ratios are high is identified by means of a coherence function, derived from spectral densities as follows:

$$\gamma^2(\omega) = \frac{\mathrm{Gxy}(\omega) \times \overline{\mathrm{Gxy}(\omega)}}{\mathrm{Gxx}(\omega) \times \mathrm{Gyy}(\omega)} \tag{1}$$

in which the overbar indicates a complex conjugate; Gxx and Gyy = power spectral densities of input (load) and output (acceleration), respectively; and Gxy = cross-spectral density, defined as follows:

$$\mathrm{Gxx}(\omega) = X(\omega)\bar{X}(\omega) \qquad \mathrm{Gyy}(\omega) = Y(\omega)\bar{Y}(\omega)$$
$$\mathrm{Gxy}(\omega) = X(\omega)\bar{Y}(\omega) \tag{2}$$

The spectral densities used in the coherency calculation are obtained as summation of the individual spectral densities of all 10 records. Fig. 14 shows a typical coherence function obtained for the dynamic tests performed at the locations shown in Table 1; the particular curve shown corresponds to the dynamic tests performed at a the main pier location (P6). For a perfectly linear system, with no presence of random noise, the coherence function should yield an ideal value of $\gamma^2 = 1$. Hence, the coherent range is identified when the coherence function is close to unity (i.e., $\gamma^2 > 0.9$).

The mobility curve, generally defined as the quotient between velocity and force in the frequency domain (Paquet and Briard 1976), is obtained for the test series as the quotient between the

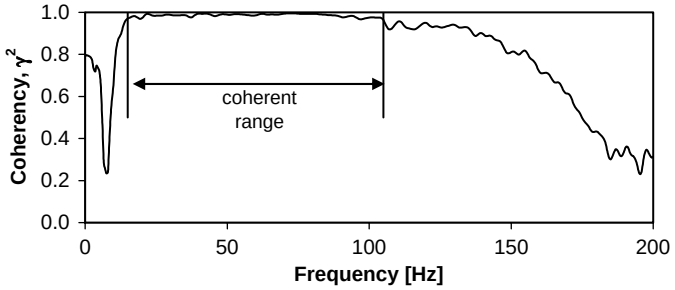

Fig. 14. Coherence function of small-strain dynamic pile test series at main pier (P6)

cross-spectral density of force and velocity and the power spectrum of the force record:

$$M(\omega) = \frac{1}{i\omega}\frac{\mathrm{Gxy}(\omega)}{\mathrm{Gxx}(\omega)} \tag{3}$$

where the $i\omega$ factor ($i^2 = -1$) is introduced in order to evaluate velocities from the acceleration records in the frequency domain. It can be shown (Paquet and Briard 1976) that the low-frequency limit of the mobility function is inversely proportional to the small-strain static stiffness K_0 and directly proportional to the circular frequency ω

$$\lim M(\omega)|_{\omega\to 0} = i\frac{\omega}{K_0} \tag{4}$$

Hence, the static stiffness is evaluated by considering the low-frequency variation of the mobility curve, within the frequency range in which results are coherent. Fig. 15 shows a typical mobility curve, for a main pier shaft (P6), in which the static stiffness is obtained by fitting a line through the origin of the curve. Hence, an accurate measurement of the initial stiffness is obtained (Caballero et al. 2003).

Table 3 shows the static stiffness evaluated by means of the dynamic tests, together with the design estimates. Measured values exceed design predictions for reduced soil stiffness as a result of installation effects. Nevertheless, the dynamic measurements show a high degree of consistency with the estimated values that consider undisturbed soil properties and the presence of underreams at the tip. Thus, the measurements indicated an adequate performance of the as-built shafts, with small-strain stiffness that exceeds design provisions.

The small-strain measurements thus provide a means of verifying the actual as-built behavior of the shafts, which can be accounted for in the construction phase of the bridge by adjusting the design stiffness accordingly.

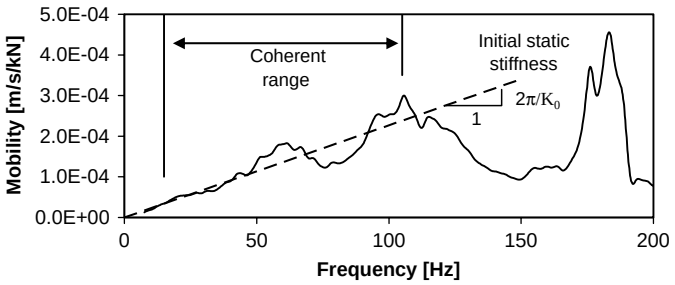

Fig. 15. Mobility function of small-strain dynamic pile test series at main pier (P6)

Table 3. Design Small-Strain Static Stiffness versus Dynamic Measurements

Piers	Reduced stiffness (kN/mm)	Intact stiffness (kN/mm)	Intact stiffness with underream (kN/mm)	Measured stiffness (kN/mm)
Main piers (P5, P6)	1,950	2,460	—	2,660
Intermediate piers (P4, P7)	2,760	3,480	3,730	3,875
Retention piers (P3, P8)	1,720	2,160	2,380	2,930
Auxiliary pier (AP11)	1,520	—	1,970	1,700
Auxiliary pier (AP15)	1,800	—	2,290	2,575

Nonlinear Finite Element Extrapolation

To obtain an estimation of the service load settlement, a nonlinear finite element (FE) model was calibrated to reproduce the initial stiffness measured by means of the dynamic tests. The nonlinear model considered hyperbolic stress-strain behavior of the soil (Caballero et al. 2003; Caballero 2006) and consisted of axis-symmetric solid elements for both the drilled shaft and the soil. The soil strengths considered in the model corresponded to the estimates made during the original design.

Caballero et al. (2003) and Caballero (2006) show that nonlinear extrapolation of small-strain measurements can provide accurate estimates of axial load–deflection curves of drilled shafts in a wide range of soil conditions, particularly for service load levels, in which the initial stiffness has a dominant influence on the behavior.

Fig. 16 shows a comparison of the nonlinear extrapolation and the design predictions on the basis of average and upper-bound $t-z$ curves with the small-strain adjustment discussed earlier. The nonlinear FE extrapolation shows a stiffer response, with settlements at a service load of 2,150 kN of 1.8–2.3 mm for the $t-z$ approximation with small-strain adjustment and 1.4 mm for the FE extrapolation.

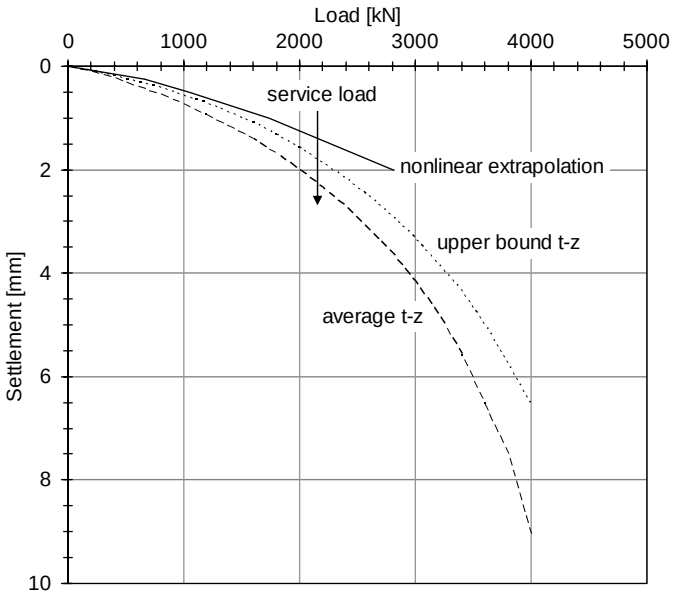

Fig. 16. Nonlinear finite element extrapolation versus design predictions at main pier (P6)

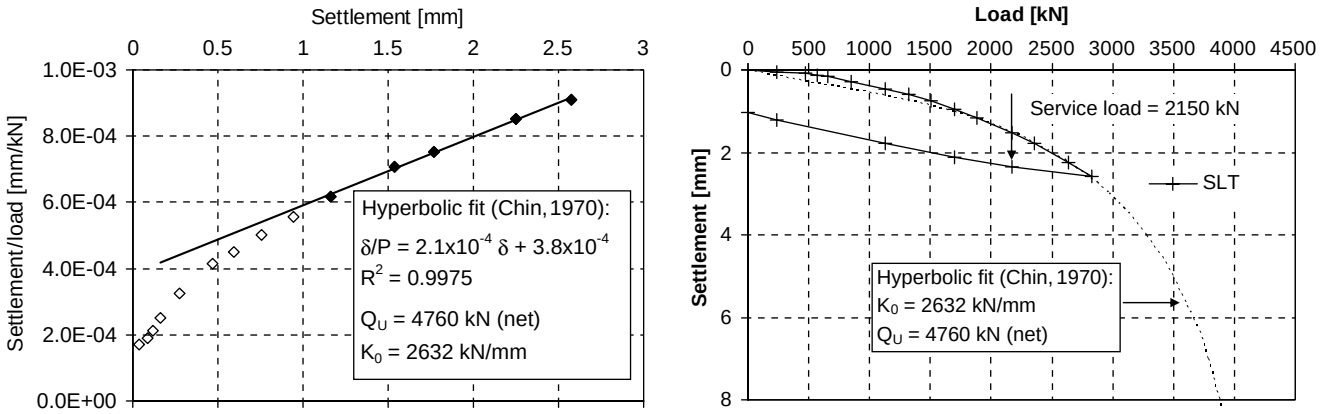

Fig. 17. Static load test results and hyperbolic extrapolation of load settlement curve at main pier (P6)

Static Load Test

A conventional SLT (ASTM 1996) was performed at a main pier location (P6) to experimentally evaluate the behavior of the shafts near the service load level. The design service load for the shaft was 2,150 kN, and the test reached a maximum load of 2,830 kN. The SLT left the shaft with a permanent settlement of 1 mm (approximately 40% of the maximum settlement reached during the test), whereas NDT does not induce any noticeable changes in the structure.

The ultimate capacity estimated in design is $Q_U = 4,470$ kN (i.e., only approximately 63% of the ultimate load is reached during the test). Thus, a hyperbolic fit proposed by Chin (1970) was used to estimate the ultimate capacity. Fig. 17 shows the test results and the hyperbolic fit, in which K_0 is the initial axial stiffness. The ultimate capacity extrapolated is approximately 7% larger than design predictions. The initial stiffness obtained by means of the hyperbolic fit is very close to the small-strain test results. However, the actual SLT results at small strains are discarded from the hyperbolic fit, because the instrumentation used to perform the test lacks accuracy within this strain range. In fact, the small-strain stiffness evaluated directly from the first few points of the SLT (i.e., without the hyperbolic fit) is found to be approximately 100% greater than that indicated by the small-strain dynamic tests.

The hyperbolic fit yields an initial stiffness almost equal to the small-strain dynamic measurements (2,632 versus $2,660$ kN/mm) and a net ultimate capacity (i.e., capacity minus the shaft weight) that slightly exceeds the design estimate (4,760 versus 4,470 kN). Hence, the SLT results, together with the hyperbolic fit, seem to match reasonably well the expected behavior of the shaft on the basis of design predictions and small-strain measurements.

Regarding settlements at the service load level, Fig. 18 shows that the SLT results indicate a settlement of 1.5 mm, whereas the nonlinear FE extrapolation shows 1.4 mm of settlement at this load. Thus, the nonlinear FE extrapolation yields a very accurate settlement estimate at this load level, consistent with previous experiences reported by Caballero et al. (2003) and Caballero (2006).

The design estimates on the basis of average and upper-bound $t-z$ curves indicate settlements of 2.3 to 1.8 mm, respectively, at the service load level. Hence, the average $t-z$ curves yield an overly conservative settlement estimate, whereas the upper-bound $t-z$ estimate is closer to the measured value but still overpredicts settlements by approximately 20%. Given the fact that the values considered in design correspond to the average $t-z$ estimates, by performing the small-strain dynamic tests and by means of the FE extrapolation a more accurate estimate of settlements can be obtained.

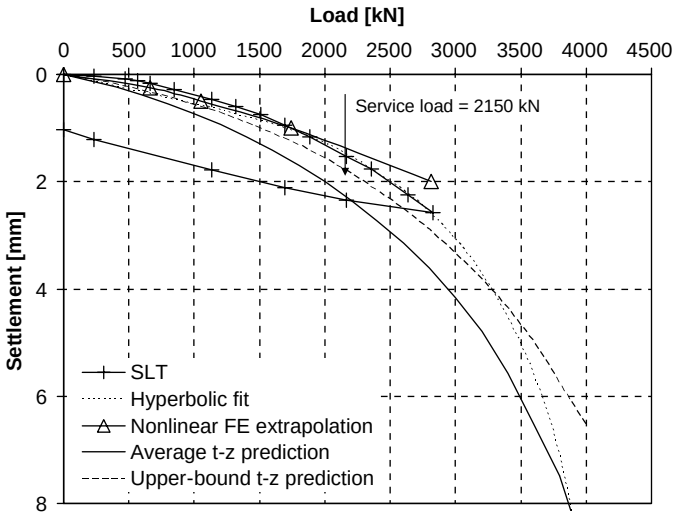

Fig. 18. Static load test results versus nonlinear finite element extrapolation and design predictions at main pier (P6)

Conclusions

The design of the Río Cuarto Bridge required an adequate characterization of the load-deflection behavior of the drilled shafts up to the service load range. To experimentally verify and adjust design predictions and to verify the integrity of the shafts, an NDT pile testing program was carried out, with a complementary large-strain SLT to verify dynamic measurements and nonlinear extrapolations into the service load range.

Small-strain results yielded stiffness for the main pier shafts that closely matches the design predictions, whereas results for other locations indicated larger stiffness than anticipated in design. Differences are partially attributed to conservative design assumptions in relation to installation effects and the presence of underreams that were not originally accounted for in the design. Other sources of difference may be attributed to spatial variability and uncertainties associated with the small-strain soil property estimation by means of the SASW method. If undisturbed soil properties are considered and underreams are accounted for, the match between prediction and measurements is greatly improved. A nonlinear FE

model was subsequently used to extrapolate small-strain results into the nonlinear range. The FE extrapolation yields service load settlements that are 20 to 40% lower than the original design predictions on the basis of upper-bound and average $t - z$ curves, respectively.

A static load test was performed at a main pier location to verify the load-deflection behavior up to service loads. Results showed that the original design estimates overpredict deflections near the service load range, whereas the nonlinear FE extrapolation of small-strain results on the basis of the technique proposed by Caballero (2006) closely matched the experimental results up to this load level. However, nonlinear extrapolation on the basis of small-strain measurements is a nondestructive technique that does not impose permanent deformations on the shafts and may be performed in the field at a fraction of the time and cost of an equivalent SLT.

For this case study, it was found that undisturbed initial stiffness of soils yields reasonable predictions of small-strain stiffness of the shafts and that load-deflection behavior in the nonlinear range on the basis of the upper-bound $t - z$ curves yields closer estimates than average $t - z$ curves. These findings are consistent with adequate construction and above-average performance of the shafts.

The NDT program was thus instrumental in verifying the behavior of the as-built shafts and the structural integrity of these elements. Small-strain results were used to adjust original conservative design predictions for initial stiffness to get a more accurate estimation of the load-deflection behavior of the as-built shafts for analysis of the structure both during construction and for long-term conditions.

References

AASHTO LRFD Bridge Design Specifications. (2008). *Customary U.S. units*, 4th Ed., AASHTO, Washington, DC. 6

ASTM. (1996). "Standard test method for piles under static axial compression load." *D1143-81*, West Conshohocken, PA.

Caballero, C. R. (2006). "Evaluación numérico experimental del comportamiento bajo carga axial de pilotes." Ph.D. thesis, Univ. Nacional de Córdoba, Córdoba, Argentina. 7

Caballero, C. R., Pinto, F., and Prato, C. A. (2003). "Load-deflection curve of drilled shafts by small strain dynamic tests coupled with nonlinear numerical model." *Proc., 12th Pan-American Conf. on Soil Mechanics and Geotechnical Engineering/Soil and Rock America 2003*, EEUU, Cambridge, MA, 1809–1816. 8 9

Chin, F. K. (1970). "Estimation of the ultimate load of piles from tests not carried to failure." *Proc., 2nd Southeast Asian Conf. on Soil Engineering*, Singapore, 91–90. 10

Paquet, J., and Briard, M. (1976). "Controle non detructif des pieux en beton." Ann. Inst. Tech. Batim. Trav. Publics, 337, 50–80. 11

Pinto, F., and Prato, C. A. (2006). "Three dimensional indirect boundary element method formulation for dynamic analysis of frames buried in semi-infinite elastic media." *J. Eng. Mech.*, 132(9), 967–978. 12

Randolph, M. F., and Wroth, C. P. (1978). "Analysis of deformation of vertically loaded piles." *J. Geotech. Engrg. Div.*, 104(GT12), 1465–1488. 13

Reese, L. C., and O'Neill, M. W. (1988). "Drilled shafts: Construction procedures and design methods." *U.S. Dept. of Transportation*, *FHWA-HI-88-042*, Dallas, USA.

Stokoe, K. H., Wright, S. G., Bay, J. A., and Roesset, J. M. (1994). "Characterization of geotechnical sites by SASW method." *Technical review: Geophysical characterization of sites, ISSMFE technical committee 10*, R. D. Woods, ed., Oxford Publishers, New Delhi, India.